Nanoscale

PAPER

View Article Online
View Journal | View Issue

Cite this: *Nanoscale*, 2017, **9**, 5194

Chemical and mechanical modulation of polymeric micelle assembly†

Nicholas E. Clay,[a] Joseph J. Whittenberg,[a] Jiayu Leong,[a] Vivek Kumar,[a] Jinrong Chen,[a] Insil Choi,[b] Evangelos Liamas,[c] Jeremy M. Schieferstein,[a] Jae Hyun Jeong,[a,b] Dong Hyun Kim,[d] Zhenyu Jason Zhang,[c] Paul J. A. Kenis,[a,e] Il Won Kim[b] and Hyunjoon Kong*[a,e]

Received 27th October 2016,
Accepted 17th March 2017

DOI: 10.1039/c6nr08414a

rsc.li/nanoscale

Recently, polymeric micelles self-assembled from amphiphilic polymers have been studied for various industrial and biomedical applications. This nanoparticle self-assembly typically occurs in a solvent-exchange process. In this process, the quality of the resulting particles is uncontrollably mediated by polymeric solubility and mixing conditions. Here, we hypothesized that improving the solubility of an amphiphilic polymer in an organic solvent *via* chemical modification while controlling the mixing rate of organic and aqueous phases would enhance control over particle morphology and size. We examined this hypothesis by synthesizing a poly(2-hydroxyethyl)aspartamide (PHEA) grafted with controlled numbers of octadecyl (C_{18}) chains and oligovaline groups (termed "oligovaline-PHEA-C_{18}"). The mixing rate of DMF and water was controlled either by microfluidic mixing of laminar DMF and water flows or through turbulent bulk mixing. Interestingly, oligovaline-PHEA-C_{18} exhibited an increased solubility in DMF compared with PHEA-C_{18}, as demonstrated by an increase of mixing energy. In addition, increasing the mixing rate between water and DMF using the microfluidic mixer resulted in a decrease of the diameter of the resulting polymeric micelles, as compared with the particles formed from a bulk mixing process. Overall, these findings will expand the parameter space available to control particle self-assembly while also serving to improve existing nanoparticle processing techniques.

Introduction

In the past 50 years, nanoparticles have been studied as carriers of various molecules for cosmetic, medical, and agricultural products.[1–4] These nanocarriers are noted for their structural stability, and can help retain the activity of multifactorial compounds.[5] Polymers can be chemically modified to tailor degradation rate and mechanism (*e.g.*, enzymatic digestion, optical trigger) and subsequent molecular release rate.[6,7] In addition, the nanoparticle surface can be chemically or physically engineered to present a desired number and type of molecules for the targeted delivery of molecular cargos.[8,9]

Polymeric micelles are typically formed by the self-assembly of amphiphilic polymers during a solvent exchange process where amphiphilic polymers are first dissolved in an organic solvent and subsequently introduced into an aqueous phase.[10–12] These polymers are typically synthesized by connecting a series of water-soluble polymers such as poly(ethylene glycol),[13] hyaluronic acid,[14] poly(2-hydroxyethyl methacrylate),[15] or polypeptides[16] with hydrophobic segments to create an amphiphilic block copolymer or graft copolymer. In aqueous media, amphiphilic polymers associate to form micelles, depending on the ratio of hydrophobic and hydrophilic domains in the polymer.[17,18]

Recently, microfluidic platforms have been considered for various nanofabrication strategies, as these devices can mix small volumes (~nL–μL) of aqueous and organic phases at controlled rates.[19–21] Microfluidic systems have been utilized previously to produce highly monodisperse populations of liposomes,[22] quantum dots,[23] and emulsions.[24] In particular, microfluidic platforms that rapidly mix solutions *via* hydrodynamic flow focusing, where a central organic solvent-polymer

[a]*Department of Chemical and Biomolecular Engineering, University of Illinois at Urbana-Champaign, Urbana, Illinois, 61801 USA. E-mail: hjkong06@illinois.edu*
[b]*Department of Chemical Engineering, Soongsil University, 369 Sangdo-ro, Dongjak-gu, Seoul 06978, Republic of Korea*
[c]*School of Chemical Engineering, University of Birmingham, Egbaston, Birmingham, UK*
[d]*Department of Human and Culture Convergence Technology R&BD Group, Korea Institute of Industrial Technology, Ansan-si Gyeonggi-do 426-910, Republic of Korea*
[e]*Carl R. Woese Institute for Genomic Biology, University of Illinois at Urbana-Champaign, Urbana, Illinois, 61801 USA*

†Electronic supplementary information (ESI) available: Additional information on synthesis of valine-NCA and polysuccinimide. Additional details on image analysis, CFD simulations, and chip preparation. Supplemental TEM images and NMR spectra. AFM and SEM images. See DOI: 10.1039/c6nr08414a

stream is sheathed by adjacent aqueous streams, have been utilized to synthesize polymeric nanoparticles, such as nanoprecipitated particles consisting of diblock copolymers.[25]

Additionally, microfluidic devices possess the potential to finely control a given set of reaction or process parameters, in turn reducing batch-to-batch variability.[26] However, there is increasing evidence that the quality of microfluidic nanoparticle assembly relies on the solubility of amphiphilic molecules in the organic phase.

With a bulk or microfluidic solvent exchange process, selection of an appropriate organic solvent is vital to: (1) ensure complete dissolution of the amphiphilic polymers and (2) retain functionality of molecular cargos. Meeting both requirements severely limits the types of polymers used as a building block for micelles and also requires efforts to seek or synthesize a good solvent *via* trial-and-error.[27] Another potentially important factor for solvent exchange is the balanced mixing of amphiphilic polymer, organic phase, and aqueous phase. For instance, amphiphilic polymers with an increased fraction of hydrophobic domains can rapidly precipitate as aggregates during the solvent exchange process prior to nanoparticle assembly. However, to date, few efforts have systematically examined and resolved these potential challenges in particle assembly.

This study therefore demonstrates the significant role of amphiphilic polymer mixing conditions in regulating polymeric micelle assembly *via* combined chemical modification of amphiphilic polymers and mechanical control of the solvent exchange process. We hypothesized that chemical modification of an amphiphilic polymer to thermodynamically improve its solubility in a given organic phase is advantageous to form nanoparticles with desired morphology and size. In addition, the microfluidic solvent exchange rate regulated by the volumetric flow rate ratio (termed FRR) between organic and aqueous phases would further mediate the self-assembly of amphiphilic polymers.

We examined this hypothesis by using a poly(2-hydroxyethyl)aspartamide (PHEA) polymer substituted with a controlled number of octadecyl chains (C_{18}) as a model amphiphilic polymer. The degree of substitution of C_{18} (DS_{C18}) was varied to create a polymeric micelle. We modified the alkylated PHEA with a controlled number of oligovaline chains to control the solubility of the polymer in an organic solvent such as dimethylformamide (DMF). The solvent exchange rate was modulated by introducing the PHEA polymers dissolved in DMF into an aqueous phase either by dropwise addition, termed off-chip or bulk mixing, or flow focusing in a microfluidic mixer, termed microfluidic or on-chip mixing, at different volumetric flow rate ratios between DMF and water (Fig. 1).

The critical role of oligovaline in improving polymer solubility was examined *via* a thermodynamic analysis. The role of oligovaline in nanoparticle formation was evaluated by quantifying the energy of mixing *via* computational simulation and experimentation. The microfluidic mixing process was also examined *via* finite element model-based simulation and microscopic visualization of flow patterns. The morphology and size of the resulting nanoparticles were evaluated with electron microscopy and atomic force microscopy (AFM). Micelle stability was further analysed *via* dynamic light scattering (DLS). Overall, this study serves to improve nanoparticle fabrication processes by expanding the parameter space available for controlled self-assembly.

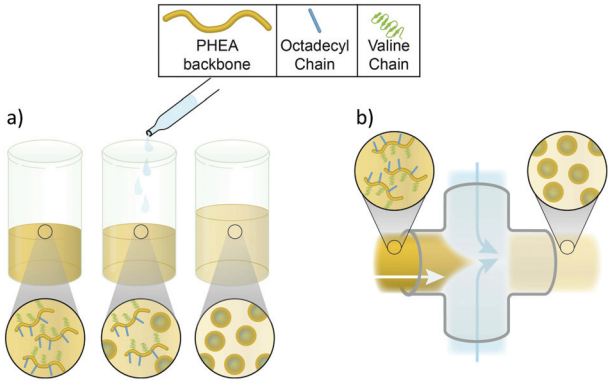

Fig. 1 Schematic depicting (a) off-chip and (b) microfluidic/on-chip mixing to prepare PHEA nanoparticles.

Results and discussion

Synthesis of oligovaline-PHEA-C_{18}

First, polysuccinimide (PSI) with an average molecular weight of 19 000 g mol^{-1} was prepared by the acid-catalysed polycondensation of aspartic acid (NMR spectrum for PSI in Fig. S1†).[28] Then, a controlled number of octadecyl (C_{18}) chains was conjugated to the PSI *via* the ring-opening nucleophilic addition of octadecylamine (Step 1 in Fig. 2). Successful conjugation of the C_{18} chain was confirmed with the peak at 0.85 ppm on the ^{1}H NMR spectrum (Fig. S2†). The remaining PSI rings were then substituted with ethanolamine and ethylenediamine (Steps 2 and 3 in Fig. 2). To quantify the degree of substitution of the C_{18} chain, eqn (1) was used.[29]

$$DS_{C_{18}} = \frac{\text{Area under peak from 0.8 to 0.94 ppm}}{(\text{Area under peak from 4.3 to 4.6 ppm}) \times 3} \quad (1)$$

Note that 3 corresponds to the number of hydrogen atoms per octadecyl chain. According to the ^{1}H NMR spectrum of the PSI substituted with C_{18}, ethanolamine, and ethylenediamine (referred to as NH_2-PHEA-C_{18}), reacting octadecylamine and PSI at a mass ratio of 0.28 resulted in DS_{C18} of approximately 20% (eqn (1)).

Separately, valine-*N*-carboxyanhydride (valine-NCA; structure and NMR spectrum in Fig. S3 and S4,† respectively) was prepared from the Fuchs–Farthing reaction.[30] In this reaction, L-valine underwent ring-closure in the presence of triphosgene, resulting in valine-NCA.[31,32] Valine-NCA reacted with the primary amines of NH_2-PHEA-C_{18}, in turn opening the valine-NCA ring. Thus, the amine served as an initiator for the polymerization of the valine groups, and an oligovaline chain

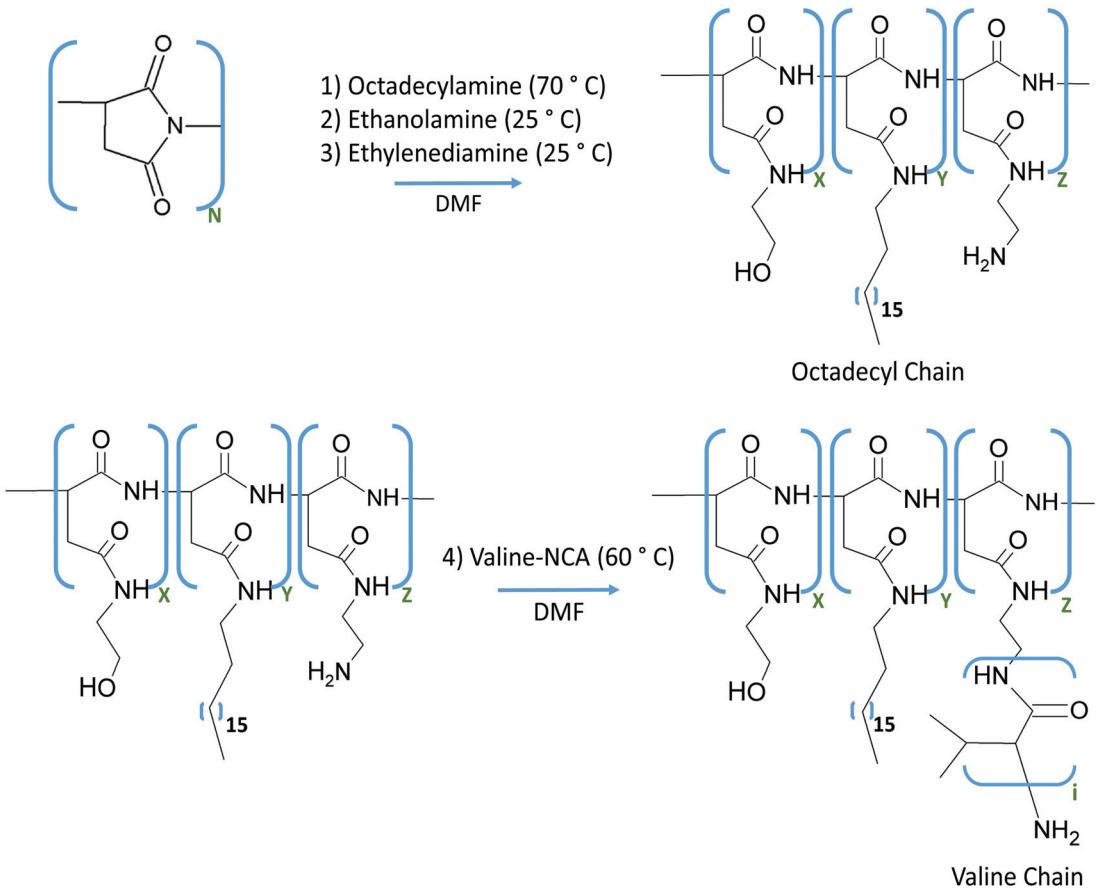

Fig. 2 Schematic depicting the synthesis of polyaspartamide substituted with octadecyl and oligovaline groups (termed "oligovaline-PHEA-C_{18}"). The molar ratio of *x*, *y*, and *z* monomers is determined by changing the mass of octadecylamine, ethanolamine, and ethylenediamine added in Steps 1, 2, and 3, respectively. Note the distribution of *x*, *y*, and *z* in the polymer chain is random.

was subsequently formed on NH_2-PHEA-C_{18} (Step 4 in Fig. 2).[33] The presence of oligovaline chains grafted to the PHEA-C_{18} was confirmed by the distinctive ^{1}H-NMR peaks at approximately 1 ppm.[34] To quantify the number ratio of valine units to PHEA units, eqn (2) was used.

$$N_{\mathrm{PHEA/val}} = \frac{\text{Area under peak from 1.01 to 1.04 ppm}}{(\text{Area under peak from 4.3 to 4.6 ppm}) \times 6} \quad (2)$$

Note that 6 corresponds to the number of protons in the isopropyl group per valine group.

The number ratio of oligovaline chains to PHEA units was approximately 1 : 100 for the oligovaline-PHEA-C_{18} with a DS_{C18} of 20%. With a quantified value for DS_{C18}, the hydrophilic mass fraction (f) of the PHEA polymer with DS_{C18} of 20% was approximated according to the following equation:

$$f = \frac{158\left(1 - \frac{DS_{C_{18}}}{100}\right)}{158\left(1 - \frac{DS_{C_{18}}}{100}\right) + 366\frac{DS_{C_{18}}}{100}}. \quad (3)$$

Note that valine, an additional hydrophobic group,[35] is neglected from this calculation due to the low number ratio of valine groups to PHEA groups. At DS_{C18} of 20%, the f of oligovaline-PHEA-C_{18} was around 0.6. Previous theoretical and experimental studies have indicated that an amphiphilic polymer with an f smaller than 0.35–0.40 self-assembles to form a polymeric vesicle.[36,37] Above this range, spherical or cylindrical micelles are typically formed. Therefore, we predicted that oligovaline-PHEA-C_{18} with DS_{C18} of 20% would form a micelle.

Solubility analysis of oligovaline-PHEA-C_{18} in DMF

We then evaluated the solubility of the synthesized amphiphilic PHEA molecules in DMF. Polymer solubility in the organic phase is a key consideration for solvent exchange, as the process involves the transitioning of the amphiphilic polymer from a region of high solubility to a region of low solubility. The information gathered in this study will also be useful for the design of other polymer systems as well. Note that some common organic solvents, such as chloroform or hexane, were not considered because the organic solvent used for self-assembly must be miscible in water in order to enable solvent exchange.

The PHEA substituted only with C_{18} chains and amine groups, termed NH_2-PHEA-C_{18}, formed a cloudy, insoluble dispersion in DMF (Fig. 3a-i). The conjugation of the oligovaline chain to NH_2-PHEA-C_{18} dramatically improved solubility of the polymer in DMF. At a DS_{C18} of 20%, a clear yellow-brown solution was made at 30 mg mL^{-1} (Fig. 3a-ii). According to measurements of polymer solubility at 0 °C, NH_2-PHEA-C_{18} (DS_{C18} = 20%) had a maximal solubility of only 7 mg mL^{-1}, while oligovaline-PHEA-C_{18} (DS_{C18} = 20%) had a maximal solubility of around 44 mg mL^{-1}.

In aqueous conditions, oligovaline-PHEA-C_{18} (DS_{C18} = 20%) has a critical micelle concentration (CMC) of 5.5 μg mL^{-1} (Fig. S5†). This CMC value is comparable to similar amphiphilic polyaspartamide polymers, further suggesting that this polymer should form micelles under different mixing conditions.[8]

To examine the underlying mechanism by which the oligovaline group improved the solubility of NH_2-PHEA-C_{18}, the thermodynamic properties related to solvation were quantified. Based on the mass of polymers dissolved in DMF at a given temperature, the Gibbs free energy change during mixing (ΔG_{mix}) was calculated using the following equation:

$$\Delta G_{mix} = -RT \ln K_{eq} \quad (4)$$

whereby R is the gas constant (8.314 J mol^{-1} K^{-1}), and T is temperature (K). K_{eq} is defined as:

$$K_{eq} = \frac{\text{Mass of PHEA polymer in solution}}{\text{Insoluble mass of PHEA polymer}}. \quad (5)$$

For the temperatures considered, ΔG_{mix} for oligovaline-PHEA-C_{18} was more negative than ΔG_{mix} for NH_2-PHEA-C_{18} (Fig. 3b). This trend suggests that the solvation of oligovaline-PHEA-C_{18} in DMF was more thermodynamically favourable than that of NH_2-PHEA-C_{18} in DMF.

Separately, using the Flory–Huggins solution theory, the entropy of mixing (ΔS_{mix}) was calculated based on the volume fraction of the oligovaline-PHEA-C_{18} or NH_2-PHEA-C_{18} dissolved in DMF:

$$\Delta S_{mix} = -R\left(\varphi_1 \ln \varphi_1 + \frac{1}{N_2}\varphi_2 \ln \varphi_2\right) \quad (6)$$

whereby φ_1 is the volume fraction of DMF, φ_2 is the volume fraction of PHEA-based polymer, and N_2 is the degree of polymerization of PHEA (approximated as 190).[38] Both oligovaline-PHEA-C_{18} and NH_2-PHEA-C_{18} have a positive entropy of mixing, suggesting a higher amount of disorder is generated as the polymer goes into solution. Interestingly, ΔS_{mix} for oligovaline-PHEA-C_{18} was approximately 3-fold larger than ΔS_{mix}

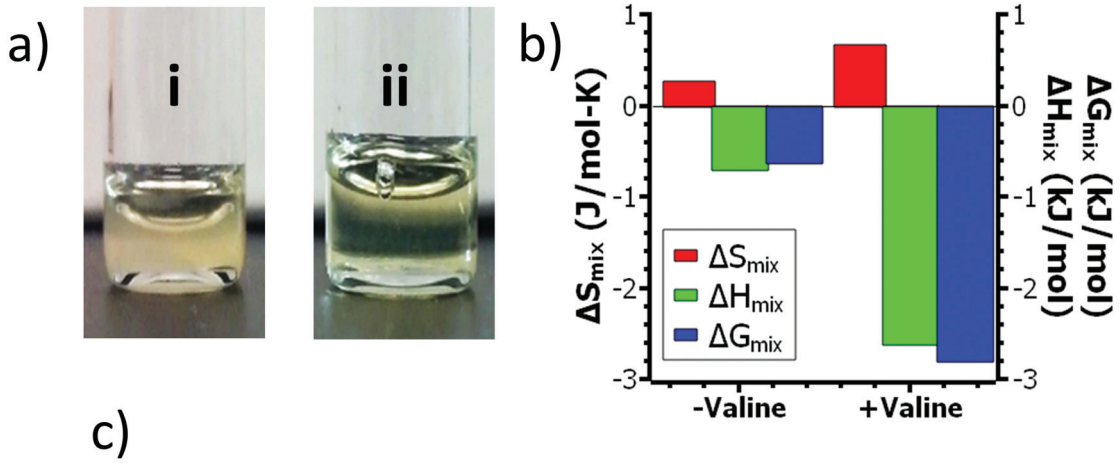

c)

Polymer with 11 units	Solvent	$\left(\frac{E_{coh}}{V}\right)_{PHEA}$ (J/cm³)	$\left(\frac{E_{coh}}{V}\right)_{S}$ (J/cm³)	$\left(\frac{E_{coh}}{V}\right)_{PHEA-S}$ (J/cm³)	$\left(\frac{\Delta E_{mix}}{V}\right)$ (J/cm³)
OH:CH_3:Valine = 8:2:1	DMF	350.2	655.7	572.9	-8.8 ± 2.6
	Water	350.2	2281.4	1698.0	4.0 ± 4.7
OH:CH_3:NH_2 = 8:2:1	DMF	436.5	655.7	595.1	-5.1 ± 3.4
	Water	436.5	2281.4	1709.4	18.5 ± 7.7

Fig. 3 Effects of oligovaline on the solubility of PHEA in DMF. (a) Images of PHEA polymers dissolved in DMF at 30 mg mL^{-1}: (i) NH_2-PHEA-C_{18} (DS_{C18} = 20%); (ii) oligovaline-PHEA-C_{18} (DS_{C18} = 20%). (b) Changes in Gibb's free energy of mixing (ΔG_{mix}; blue), the heat of mixing (ΔH_{mix}; green), and the entropy of mixing (ΔS_{mix}; red) for oligovaline-PHEA-C_{18} (DS_{C18} = 20%; termed "+valine") and NH_2-PHEA-C_{18} (DS_{C18} = 20%; "–valine"). All values represent the average of values obtained at three different temperatures (–20, 0, or 25 °C). (c) The computational simulated energy of mixing per unit volume for the oligovaline-PHEA-C_{18} and the NH_2-PHEA-C_{18} with 11 units dissolved in DMF or water at 30 vol%.

for NH_2-PHEA-C_{18} (Fig. 3b). This increase in ΔS_{mix} is likely due to the higher total fraction of PHEA polymer solubilized for oligovaline-PHEA-C_{18} than that for NH_2-PHEA-C_{18}. The enthalpy of mixing (ΔH_{mix}) was approximated based on ΔG_{mix} (eqn (4)) and ΔS_{mix} (eqn (7)):

$$\Delta H_{mix} = \Delta G_{mix} + T\Delta S_{mix}. \quad (7)$$

According to the calculation, the negative ΔH_{mix} was approximately 3-fold higher than ΔH_{mix} for NH_2-PHEA-C_{18} (Fig. 3b). This increase in the enthalpy of mixing is likely due to the changes in intermolecular interactions between PHEA polymer and DMF that occur when the oligovaline chain is conjugated onto the polymer backbone.

Molecular simulation of oligovaline-PHEA-C_{18} and NH_2-PHEA-C_{18} solubility

To further examine the role of the oligovaline groups on polymer solubility, the energy of mixing per unit volume ($\Delta E_{mix}/V$) of the model PHEA polymer with 11 repeating units was computationally calculated as follows.[39]

$$\frac{\Delta E_{mix}}{V} = \phi_{PHEA}\left(\frac{E_{coh}}{V}\right)_{PHEA} + \phi_{SDMF}\left(\frac{E_{coh}}{V}\right)_{S} - \left(\frac{E_{coh}}{V}\right)_{PHEA-S} \quad (8)$$

Here, ϕ_{PHEA} and ϕ_S are volume fraction of the PHEA-based polymer and solvent (*i.e.*, DMF or water), respectively. $(E_{coh}/V)_{PHEA}$ $(E_{coh}/V)_S$, and $(E_{coh}/V)_{PHEA-S}$ are the cohesive energy density values of pure PHEA, solvent, and PHEA in the solvent, respectively. For all polymers including oligovaline-PHEA-C_{18} and NH_2-PHEA-C_{18}, the negative energy of mixing indicates that DMF is a better solvent than water (Fig. 3c). Also, oligovaline-PHEA-C_{18} exhibited a more negative energy of mixing, thus indicating a higher solubility in DMF and, furthermore, confirming the results obtained experimentally. While the scope of the MD simulation was limited to a polymer with 11 repeating units for ease of computation (molecular structure in Fig. S6†), the computational results suggested that the oligovaline chain plays an important role in increasing the solubility of PHEA in DMF.

We propose that this improved solubility of the oligovaline-PHEA-C_{18} is due to enhanced intermolecular association between the polymer and DMF. The amide groups of the oligovaline chains coupled to the NH_2-PHEA-C_{18} likely formed hydrogen bonds with DMF, a hydrogen bond acceptor (Fig. 4). Thus, the oligovaline groups coupled to PHEA increased the number of hydrogen bonds between polymers and DMF, thus improving solubility.[40] Without this additional hydrogen bonding, van der Waals interactions between the octadecyl chains drove polymer–polymer association, resulting in insoluble aggregates.[41]

At higher DS_{C18} values (*e.g.*, 40%) and lower DS_{C18} (*e.g.*, 0%), the addition of an oligovaline chain results in high PHEA solubility in DMF (Fig. S7 and Table S1†), suggesting that this chemistry has additional utility for future polymer systems. The observed polymer solubility for a library of different poly-

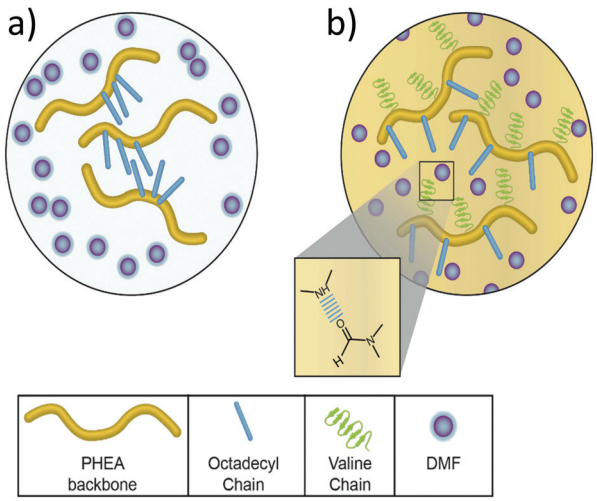

Fig. 4 Proposed mechanism for the solubility changes that occur upon the conjugation of the oligovaline chains to NH_2-PHEA-C_{18}. (a) Without the oligovaline chains, the PHEA polymer associates with itself, yielding insoluble aggregates. (b) By conjugating oligovaline chains to NH_2-PHEA-C_{18}, additional sites for hydrogen bonding with DMF are present in the polymer, thus improving its solubility in DMF. The dashed blue line (see inset) indicates the presence of hydrogen bonding between secondary amines on the valine chain and DMF.

aspartamide polymers is reported in Table S1.† Taken together, these broad improvements in polymer solubility suggest that the presence of oligovaline chains can increase the solubility of different PHEA molecules in organic solvents.

Determining mixing efficiency of the microfluidic mixer

Separately, a PDMS microfluidic mixer was prepared, with a port for an aqueous phase (marked with **A** in Fig. 5) and a port for the DMF phase containing amphiphilic PHEA polymers (**D** in Fig. 5). The DMF solution and the aqueous phase were mixed at different ratios starting at the flow focusing junction (zoomed-in region depicted in Fig. 5c). Here, the volumetric flow rate of the aqueous phase to the volumetric flow rate of the DMF phase was denoted as the flow rate ratio (FRR). The mixed solution then travelled through a straight channel followed by a curved channel to a single outlet (marked with **O** in Fig. 5a) where the PHEA–DMF–water mixture was collected. All experiments and computational on-chip studies examined FRR at 5, 10, and 20, with a constant total volumetric flow rate of 140 μL min^{-1}.

CFD simulations to evaluate microfluidic mixing

Experimentally quantifying diffusive mixing of flow focusing systems with two different solvents is particularly challenging due to changes in fluid viscosity, diffusion coefficient, and fluid velocity profile as a function of channel length.[42] Therefore, CFD simulations were conducted to qualitatively examine the mixing of DMF and water in the microfluidic device. One key parameter that determines the mixing con-

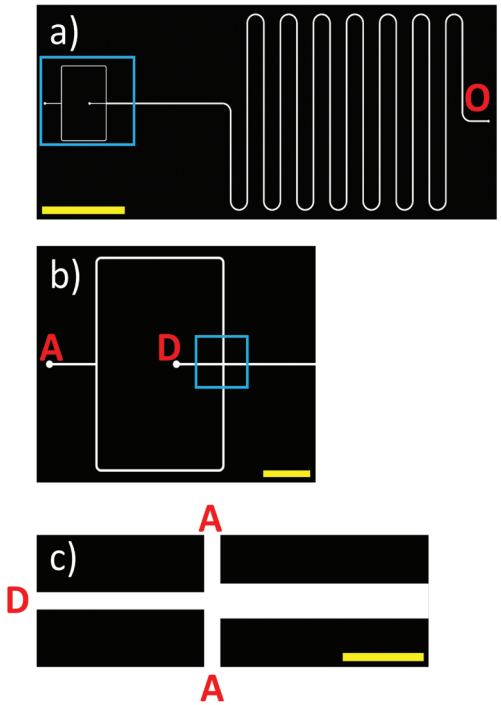

Fig. 5 (a) CAD image of the entire microfluidic mixer design. "O" corresponds to the outlet for the mixed DMF/water streams. A region of interest (depicted in b) is denoted with a blue box. The yellow scale bar corresponds to 1 cm. (b) Zoomed-in image of the inlets of the chip. "D" corresponds to the inlet stream for DMF with dissolved polymer, and "A" corresponds to the inlet stream for the aqueous media. A region of interest (termed flow focusing region; depicted in c) is denoted with a blue box. Yellow scale bar corresponds to 2 mm. (c) Zoomed-in image of the flow focusing region. The yellow scale bar corresponds to 0.5 mm.

ditions on-chip is FRR, which directly impacts the diameter of the central focused stream and therefore affects diffusion rate (*i.e.*, thinner focused streams mix faster). Here, we performed 2-D CFD simulations of three different FRRs (5, 10, and 20) utilizing a shorter version of the microfluidic platform, but with identical channel widths. The CFD simulation was run using the Naviér-Stokes equation (eqn (S1) and (S2)†) and the convective-diffusion equation (eqn (S3)†). For all FRR values, the Reynold's number (eqn (S4)†) was constant at around 14, thus indicating that all microfluidic mixing will be done in a laminar region. In contrast, the Reynold's number for off-chip mixing (eqn (S5)†) is over 3000, suggesting a mostly turbulent mixing regime.[43]

CFD simulations indicate the central focused stream narrowed slightly as FRR increased (Fig. 6a). Thinner organic streams lead to more rapid solvent exchange, thus suggesting a faster mixing rate. In addition, the role of FRR on the mixing of DMF and water was experimentally examined by using DMF mixed with a colorant. As FRR increased from 5 to 10 and 20, the initial diameter of the DMF stream in the aqueous phase became increasingly smaller, as determined with brightfield images (Fig. 6b). For FRR-5, the DMF stream diameter was 50 μm. At FRR-10 and FRR-20, the DMF stream diameter reduced to 36 and 29 μm, respectively.

Based on the computational and experimental quantification of mixing conditions on-chip, the mixing rate of DMF with water is slowest for FRR-5, as determined by the thickness of the organic stream in water. Similarly, the DMF concentration past the flow focusing region was noticeably higher when compared to similar regions in the FRR-10 and FRR-20 conditions (Fig. 6a). Based on these observations, it is likely that the high DMF concentration (13% by volume when fully mixed in water) at FRR-5 potentially leads to a heterogeneous micelle population. Therefore, on-chip mixing was performed only at FRR-10 and FRR-20, whereby the final DMF concentration is 10% by volume or less in a fully-mixed condition. We anticipated that micelle self-assembly would occur under more homogenous solvent conditions if the final DMF concentration is within this range, in turn leading to a monodisperse population of micelles.

Polymeric micelle assembly

PHEA solutions were injected into the microfluidic chip at different FRR values while keeping total volumetric flow rate constant. In particular, DMF dissolved with the oligovaline-PHEA-C_{18} with DS_{C18} of 20% was mixed with the aqueous phase at FRR of 10 and 20. Separately, the aqueous phase was introduced into the DMF-polymer solution dropwise in order to prepare micelles *via* off-chip precipitation. Independent of FRR and particle assembly process, oligovaline-PHEA-C_{18} formed a micelle, as confirmed with TEM images (Fig. 7).

Interestingly, the average diameter of the micelles prepared with the microfluidic mixer ranged from 100 to 200 nm, while the average diameter of the micelles prepared with the off-chip precipitation was around 300 ± 130 nm. More interestingly, as FRR increased from 10 to 20, the micelle diameter decreased from 190 ± 60 nm to 100 ± 40 nm (Fig. 8). In addition, solutions of oligovaline-PHEA free of C_{18} chains and solutions of NH_2-PHEA-C_{18} did not form micelles with off-chip mixing (Fig. S8a and S8b†), suggesting that both a high degree of hydrophobicity (from the octadecyl chains) and a high solubility in the organic solvent (from the oligovaline group) is necessary for self-assembly in a DMF/water solvent exchange.

These differences in micelle sizes can be explained by comparing the rate at which DMF and water mix with the rate at which polymer chains self-assemble to form a micelle. As confirmed with computational simulations and experimental visualizations, an increase in FRR increases the mixing rate of DMF and water. It is therefore likely that the C_{18} chains of oligovaline-PHEA-C_{18} should be driven to self-associate to form the micelle core more quickly at the higher FRR, thus resulting in the micelles with a smaller diameter.[44] This trend was confirmed with micelle images captured with scanning electron microscopy and atomic force microscopy (Fig. S10 and S11†). Note that AFM captures the particles in a hydrated state while SEM and TEM image the particles in a dried state. Therefore, the micelles imaged with electron microscopes likely collapsed and subsequently expanded on the solid support by the high

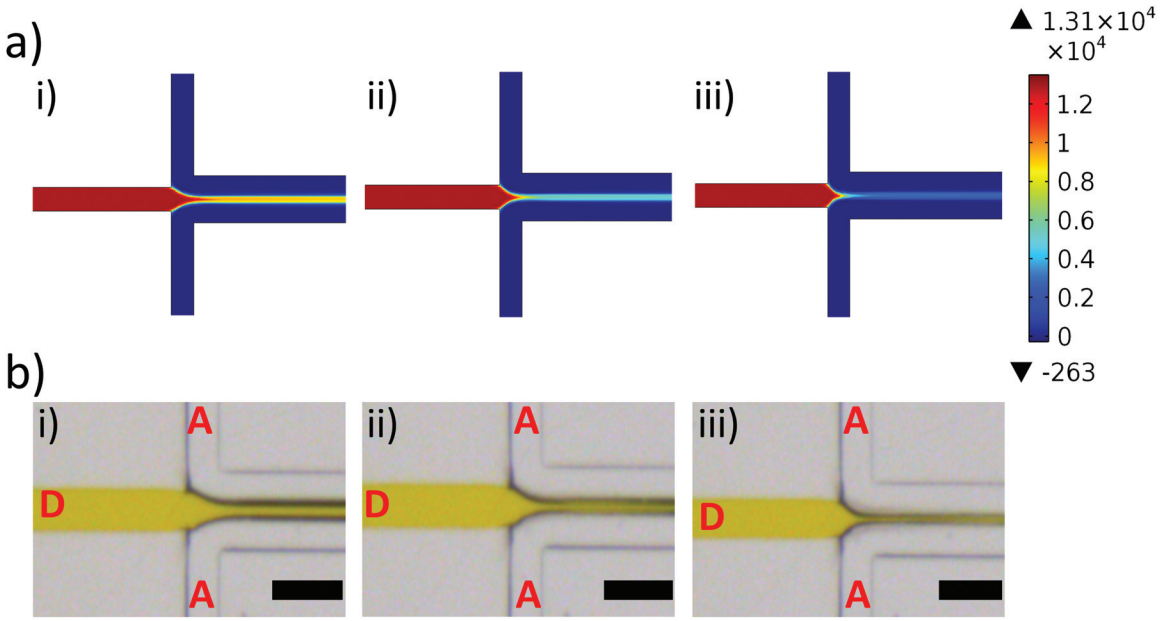

Fig. 6 Computational and experimental determination of flow conditions on-chip. (a) CFD-generated concentration profiles depicting DMF and water concentrations on-chip. The colour legend indicates DMF concentration (mol m^{-3}), red corresponds to a high DMF concentration, and blue corresponds to a low DMF concentration. CFD simulations were run for FRR-5 (i), FRR-10 (ii), and FRR-20 (iii). (b) Brightfield microscope images of the chip in operation. A yellow food colorant was used to distinguish the DMF stream (labelled "D") from the aqueous stream (labelled "A"). The flow rate ratio (FRR) varies from 5 (i) to 10 (ii) and 20 (iii). The black scale bar corresponds to 200 μm.

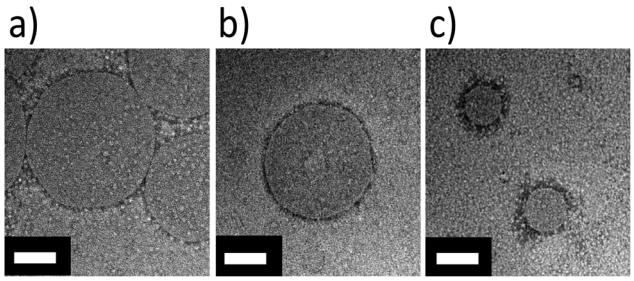

Fig. 7 TEM images of PHEA micelles. Oligovaline-PHEA-C_{18} (DS_{C18} = 20%) micelles formed with off-chip mixing (a), with microfluidic mixer at FRR-10 (b), and with microfluidic mixer at FRR-20 (c). The white scale bars represent 100 nm. Additional TEM images are available for reference in Fig. S9.†

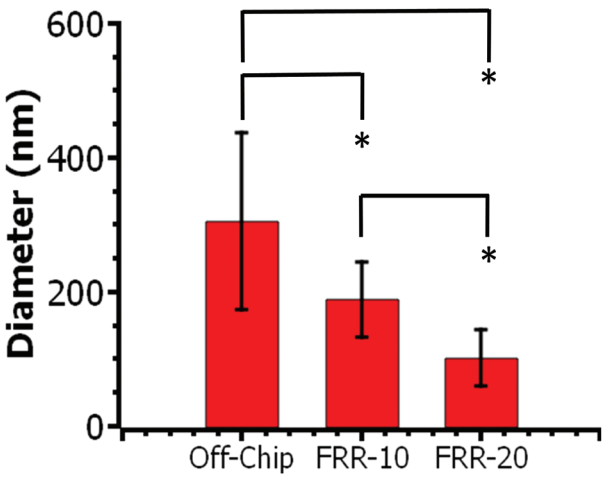

Fig. 8 Diameter of oligovaline-PHEA-C_{18} (DS_{C18} = 20%) micelles quantified with TEM images. At least 15 particles were analysed per condition. * represents the statistical significance of the difference between conditions (*p < 0.05). Values and bars correspond to averages and standard deviation of one set of size measurements, respectively.

vacuum pressure, thus making the nanoparticles appear slightly larger.

Lastly, the long-term stability of the micelles was analysed using dynamic light scattering (DLS) (Fig. S12†). Interestingly, the micelles prepared at FRR-10 underwent a decrease in hydrodynamic diameter within a day. Then, the particle size remained constant over a week. The micelles prepared at FRR-20 exhibited a minimal change in size over 1 week. This change in micelle stability can be understood by considering the kinetics of microfluidic mixing.

In the microfluidic system, the polymer transitions from a good solvent condition (*i.e.*, DMF) to a poor solvent condition (*i.e.*, water) and self-assembles into a micelle. This process takes place at different rates based on the FRR, and it is likely that the microfluidic mixing process kinetically traps micelles at different non-equilibrium states.[45] The micelles would then slowly transition to an equilibrium state over the course of several days. This journey to equilibrium is likely reflected in the Fig. S12,† as the micelles prepared at FRR-10 and FRR-20 converge to the same (equilibrium) size over several days. It may be possible to permanently trap the micelles at a non-

equilibrium state (*i.e.*, the day 0 size) by covalently crosslinking the hydrophobic domains in the micelle, similar to previously reported protocols.[46]

Conclusions

In conclusion, tuning of the solubility of the amphiphilic polymers in an organic phase and use of a laminar flow-based microfluidic mixing process enables regulating the size of polymeric micelles. The oligovaline groups conjugated to the NH_2-PHEA-C_{18} contributed to thermodynamically improving the solubility of the polymer in DMF, likely due to increased hydrogen bonds between polymer and DMF. Moreover, the microfluidic mixer enabled us to mix laminar streams of DMF and water at controlled rates. Subsequently, increasing the mixing rate in the microfluidic mixer decreased the size of micelles formed by the oligovaline-PHEA-C_{18} with DS_{C18} of 20%. Eventually, the micelles would transition to a size around 80 nm, based on a long-term DLS study. We envision that additional modifications to oligovaline-PHEA-C_{18} can help improve long-term micelle stability.

This study demonstrates the importance of polymer solubility in microfluidic-based solvent exchange process. Although several studies examined the role of microfluidic mixing on nanoparticle assembly, the importance of polymer solubility in controlling particle morphology and size was not addressed. The approach we articulated herein will widen the parameter space used for nanoparticle self-assembly.

Experimental

All chemicals were purchased from Sigma-Aldrich and used without purification, unless otherwise noted. Unless noted, all water was high-pressure liquid chromatography (HPLC) grade water (Macron).

Synthesis of NH_2-PHEA-C_{18}

First, 291 mg of polysuccinimide (termed PSI; synthesis details in ESI†) was dissolved in DMF (ACS grade) at a concentration of 20–25 mg mL^{-1}. Then, 81 or 162 mg of octadecylamine was added to the reaction mixture to form PHEA-C_{18} with a degree of substitution of octadecyl chains (DS_{C18}) of 20%. After reaction for at least 12 hours under nitrogen at 70 °C, the reaction mixture was cooled to room temperature. Then, 161 μL (for DS_{C18} of 20%) of ethanolamine was added dropwise and then reacted for another 24 h. Afterward, a dilute solution of excess ethylenediamine was prepared in dry DMF. Then, the reaction mixture was slowly added to the ethylenediamine solution over several minutes. For this step of the reaction, the molar ratio of ethylenediamine to unreacted PSI rings was at least 5 : 1. After reacting for 3 hours at room temperature, the reaction mixture was dialyzed for at least 2 days against DI water (MWCO 12 000–14 000, Fisherbrand), frozen, and then lyophilized to form a dry powder (Labconco).

Synthesis of oligovaline-PHEA-C_{18}

First, 165 mg of NH_2-PHEA-C_{18} with DS_{C18} of 20% was separately dissolved in 3 mL DMF, and then slowly heated to 60 °C. In parallel, 29 mg of valine-*N*-carboxyanhydride (valine-NCA; synthesis details and structure in ESI†) were dissolved in 1 mL of DMF. This solution was then added dropwise to the mixture of NH_2-PHEA-C_{18} with DS_{C18} of 20%. After reacting at 60 °C for at least 24 h under nitrogen, the reaction mixture was dialyzed (MWCO 3500, Fisherbrand) against DI water for at least 2 days, while changing water at least three times. The sample was then frozen and lyophilized to form a dry powder (Labconco).

NMR analysis of PSI, valine-NCA, and oligovaline-PHEA-C_{18}

All polymers were dissolved in dimethyl sulfoxide-d_6 (Cambridge Isotope Laboratories) at a concentration of at least 10 mg mL^{-1}, and then loaded into an NMR tube (Varian VXR 500). To improve the height of the analyte peaks, solvent saturation was used as needed. All scans were done at 35 °C, and at least 15–20 scans were taken per sample. All spectra were processed with ACDLABS 12.0 software.

Measurement of critical micelle concentration

Oligovaline-PHEA-C_{18} was dispersed in water at a range of concentrations from 0 to 1 mg mL^{-1}. At least 3 mL of each polymer dispersion was prepared in a glass vial. Then, 30 μL of a pyrene solution in acetone was added to each vial (final concentration: 6.16×10^{-7} M). Acetone was evaporated overnight in a fume hood. The polymer solution was excited from 300 to 360 nm, and the emission wavelength was collected at 395 nm. Both the emission and excitation bandwidths were set to 2.5 nm in order to obtain a smooth curve. An intensity ratio at two separate peaks (337 nm and 334 nm) in the excitation spectra (defined as $I_{337\ nm}/I_{334\ nm}$) was plotted *versus* polymer concentration and then fitted to two separate linear curves. When pyrene is placed in a hydrophobic environment, this intensity ratio increases. The critical micelle concentration (CMC) was defined as the inflection point in the resulting curve, as previously reported.[8]

Molecule dynamics simulation of PHEA solubility

Molecular dynamics (MD) simulations were employed to study the effect of the oligovaline chains on the solubility of NH_2-PHEA-C_{18} and oligovaline-PHEA-C_{18}. All computational calculations were performed using Materials Studio simulation software (version 8.0) from BIOVIA equipped with COMPASS II force field.[47] Coulomb interactions were calculated using Ewald summation, and van der Waals interactions were determined using an atom-based summation method (15.5 Å cut-off distance). Two model polymers with 11 units were examined, with side chain compositions of (i) hydroxyethyl : C_{18} : aminoethyl = 8 : 2 : 1 (for NH_2-PHEA-C_{18}), and (ii) hydroxyethyl : C_{18} : oligovaline = 8 : 2 : 1 (for oligovaline-PHEA-C_{18}) (Fig. S1†). The cohesive energy densities of pure polymers, solvents (DMF or water), and polymers in solvents were obtained through the MD simulation to ultimately

calculate the energy of mixing per unit volume. A polymer concentration of 30 vol% was selected. Each model polymer was first optimized using Forcite module, and the optimized structure was packed into a lattice typically *ca.* (50 Å)^3 (density 1 g cm^{-3}) using the Amorphous Cell module. Once the lattice was energetically minimized, MD method was implemented for 100 ps with 1 fs time step. The NVT ensemble (Nosé thermostat) was used at 298 K (Q ratio: 0.01).[48] The initial 50 ps was for equilibration, and the later 50 ps was for data sampling at 10 ps interval. MD calculations were similarly performed for pure solvents and polymers with 11 units (30 vol%) in solvents. Each case was simulated at least three times starting from independent initial structures, and the lowest energy result was chosen for the sampling of five structures. The reported values of cohesive energy density and the energy of mixing per unit volume were the average from five sampled structures.

Determination of maximal solubility of PHEA

Information on the labelling of PHEA polymers with fluorescein isothiocyanate (FITC) is included in ESI.† Oligovaline-PHEA-C_{18} and NH_2-PHEA-C_{18} labelled with FITC were dissolved in DMF at varying concentrations ranging from 0 to 250 μg mL^{-1}. Then, a linear calibration curve was established for each polymer functionalized with FITC by measuring polymer concentration *versus* the fluorescence intensity at 485 nm (Tecan Infinite 200 PRO plate reader; gain set to 50). To determine the maximal solubility of oligovaline-PHEA-C_{18} and NH_2-PHEA-C_{18}, a mass of polymer (5–15 mg) was placed in a clean glass scintillation vial, and then dissolved at a given concentration (50 mg mL^{-1} for oligovaline-PHEA-C_{18}, or 15 mg mL^{-1} for NH_2-PHEA-C_{18}). Then, the vial was mechanically agitated briefly, then incubated for 1 h at −20, 0, or 25 °C. After incubation, the polymer solution was separated from the insoluble polymer with centrifugation (two minutes at 10 000 rcf; Eppendorf centrifuge 5424). The mass of insoluble polymer was then dissolved in a large volume of DMF overnight at room temperature in the dark, and the fluorescent intensity of the resulting solution was then taken at 485 nm. The concentration of soluble and insoluble polymer was then back-calculated using the established calibration curve and a mass balance equation.

COMSOL simulation of microfluidic flow conditions

Two-dimensional computational fluid dynamics (CFD) simulations of flow focusing experiments were performed on COMSOL Multiphysics software (v5.1). Details are described in the ESI.†

Preparation of PHEA nanoparticles using the microfluidic mixer

Oligovaline-PHEA-C_{18} (DS_{C18} of 20%) was dissolved in DMF at a concentration of 30 mg mL^{-1}. A 1 mL glass syringe containing 300 μL of the PHEA polymer solution was loaded onto a microliter syringe pump (Harvard Apparatus). Separately, a syringe charged with 10 mL of phosphate buffered saline (PBS, Corning Cellgro) was loaded onto a millilitre syringe pump (Harvard Apparatus). For both solutions, care was taken to remove air bubbles. Prior to use, microfluidic chips were flushed with isopropanol and then PBS at a flow rate of 30 μL min^{-1} to remove any air pockets. Then, PBS and oligovaline-PHEA-C_{18} in DMF were pumped through the chip at the following flow rates: 117 μL of PBS per min: 23 μL of DMF solution per min (FRR-5); 127 μL of PBS per min: 13 μL of DMF solution per min (FRR-10); 133 μL of PBS per min: 7 μL of DMF solution per min (FRR-20). The outlet from the tube was collected in a centrifuge tube. Afterwards, the nanoparticles were washed twice in a 0.5 mL centrifugal filter (100 000 MWCO; Amicon Millipore) at 1500 rcf for at least 10 minutes (Eppendorf centrifuge 5424), and each time re-dispersed in water. In order to visualize the mixing conditions on-chip, the experiments described above were repeated, but with DMF containing an orange-red food colorant (McCormick). All images were captured with a light microscope (Leica M205 C).

Off-chip preparation of PHEA nanoparticles

Separately, 100 μL of oligovaline-PHEA-C_{18} solution was added into a 7 mL scintillation glass vial, and then stirred with a magnetic stir bar (12.7 mm diameter) at 1000 rpm on a stirring plate. Then, 1 mL of PBS was added in a drop-wise fashion to the PHEA solution over the course of approximately 15 to 30 seconds. The resulting particles were then washed in the same manner as the particles prepared on the microfluidic mixer.

TEM imaging of PHEA nanoparticles

PHEA nanoparticles were suspended in water at 0.75–1.5 mg mL^{-1}. Separately, a 20 mg mL^{-1} solution of phosphotungstic acid (PTA) was prepared and the pH was adjusted to a neutral range (6–8) with concentrated NaOH. Then, the PTA solution and the particle dispersions were mixed in a 1 : 1 volumetric ratio. Approximately 10 μL of this solution was quickly added to a 200 mesh carbon TEM grid (EMS) on top of a filter paper, and then dried in air for about 20 minutes before imaging. Images were captured (JEOL 2100) at 200 kV, with multiple images taken on at least three different sections of each grid. All images were analysed in ImageJ (NIH). Approximately 13 to 20 nanoparticles were analysed per condition. To analyse the diameter of the oligovaline-PHEA-C_{18} micelle, a straight line was drawn across the micelle image and then measured.

Nanoparticle stability test using dynamic light scattering (DLS)

Micelle size was analysed using a Zetasizer Nano ZS (Malvern Instrument Ltd) equipped with a He–Ne laser beam at 633 nm (scattering angle: 173°) over 7 days. The concentration of the micelles was 0.75 mg mL^{-1}. Each sample was measured three times, and an average micelle size was obtained.

Statistical analysis of data

Statistical significance between all conditions was compared using a one-way ANOVA test with a *post-hoc* Tukey's test (R Studio 3.2.2).

Acknowledgements

Electron microscopy and dynamic light scattering was carried out in part in the Frederick Seitz Materials Research Laboratory Central Facilities, University of Illinois. Work was funded by the National Institutes of Health (1R01 HL109192 to H. J. K.) and partially by Korea Institute of Industrial Technology (JE 140004 to H. K.). N. C. was supported by a Dow Graduate Fellowship and a DuPont Graduate Fellowship. The manuscript was written with the contributions of all authors. N. C. and H. K. designed the experiments, analyzed data, and developed the major conclusions. J. W., V. K., J. S., and P. K. provided microfluidic designs, chips, and expertise. J. C., J. H., and J. L. optimized polymer synthesis. I. K. and I. C. helped run computational simulations. D. K. provided insights during manuscript preparation. E. L. and Z. J. Z. assisted with AFM measurements.

Notes and references

1 L. Taborga, K. Díaz, A. F. Olea, P. Reyes-Bravo, M. E. Flores, H. Peña-Cortés and L. Espinoza, *J. Agric. Food Chem.*, 2015, **63**, 6890–6896.
2 X. Xu, X. Ni, Y. Cao, X. Zhuo, X. Yang and G. Cao, *Electrophoresis*, 2014, **35**, 827–835.
3 P. A. Spagnuolo, D. G. Dalgleish, H. D. Goff and E. R. Morris, *Food Hydrocolloids*, 2005, **19**, 371–377.
4 D. H. Levine, P. P. Ghoroghchian, J. Freudenberg, G. Zhang, M. J. Therien, M. I. Greene, D. A. Hammer and R. Murali, *Methods*, 2008, **46**, 25–32.
5 M.-C. Jones and J.-C. Leroux, *Eur. J. Pharm. Biopharm.*, 1999, **48**, 101–111.
6 Y. Shao, C. Shi, G. Xu, D. Guo and J. Luo, *ACS Appl. Mater. Interfaces*, 2014, **6**, 10381–10392.
7 P. S. Kulkarni, M. K. Haldar, R. R. Nahire, P. Katti, A. H. Ambre, W. W. Muhonen, J. B. Shabb, S. K. R. Padi, R. K. Singh, P. P. Borowicz, D. K. Shrivastava, K. S. Katti, K. Reindl, B. Guo and S. Mallik, *Mol. Pharmaceutics*, 2014, **11**, 2390–2399.
8 M.-H. Lai, N. E. Clay, D. H. Kim and H. Kong, *Nanoscale*, 2015, **7**, 6737–6744.
9 F. Meng, G. H. M. Engbers and J. Feijen, *J. Controlled Release*, 2005, **101**, 187–198.
10 K. Vijayakrishna, D. Mecerreyes, Y. Gnanou and D. Taton, *Macromolecules*, 2009, **42**, 5167–5174.
11 C. Houga, J. Giermanska, S. Lecommandoux, R. Borsali, D. Taton, Y. Gnanou and J.-F. Le Meins, *Biomacromolecules*, 2009, **10**, 32–40.
12 H. R. Marsden, L. Gabrielli and A. Kros, *Polym. Chem.*, 2010, **1**, 1512–1518.
13 F. Ahmed and D. E. Discher, *J. Controlled Release*, 2004, **96**, 37–53.
14 E. Saadat, M. Amini, R. Dinarvand and F. A. Dorkoosh, *J. Appl. Polym. Sci.*, 2014, **131**, 40944.
15 R. P. Johnson, Y.-I. Jeong, E. Choi, C.-W. Chung, D. H. Kang, S.-O. Oh, H. Suh and I. Kim, *Adv. Funct. Mater.*, 2012, **22**, 1058–1068.
16 L. Zhao, N. Li, K. Wang, C. Shi, L. Zhang and Y. Luan, *Biomaterials*, 2014, **35**, 1284–1301.
17 R. Nagarajan, *Langmuir*, 2002, **18**, 31–38.
18 L. Maibaum, A. R. Dinner and D. Chandler, *J. Phys. Chem. B*, 2004, **108**, 6778–6781.
19 C.-Y. Lee, C.-L. Chang, Y.-N. Wang and L.-M. Fu, *Int. J. Mol. Sci.*, 2011, **12**, 3263–3287.
20 J. C. Stachowiak, D. L. Richmond, T. H. Li, A. P. Liu, S. H. Parekh and D. A. Fletcher, *Proc. Natl. Acad. Sci. U. S. A.*, 2008, **105**, 4697–4702.
21 G. M. Whitesides, *Nature*, 2006, **442**, 368–373.
22 S. M. Phapal and P. Sunthar, *Chem. Phys. Lipids*, 2013, **172–173**, 20–30.
23 Z.-H. Tian, J.-H. Xu, Y.-J. Wang and G.-S. Luo, *Chem. Eng. J.*, 2016, **285**, 20–26.
24 R. K. Shah, H. C. Shum, A. C. Rowat, D. Lee, J. J. Agresti, A. S. Utada, L.-Y. Chu, J.-W. Kim, A. Fernandez-Nieves, C. J. Martinez and D. A. Weitz, *Mater. Today*, 2008, **11**, 18–27.
25 R. Karnik, F. Gu, P. Basto, C. Cannizzaro, L. Dean, W. Kyei-Manu, R. Langer and O. C. Farokhzad, *Nano Lett.*, 2008, **8**, 2906–2912.
26 T. W. Phillips, I. G. Lignos, R. M. Maceiczyk, A. J. deMello and J. C. deMello, *Lab. Chip*, 2014, **14**, 3172.
27 Y. Lu and K. Park, *Int. J. Pharm.*, 2013, **453**, 198–214.
28 M. Tomida, T. Nakato, M. Kuramochi, M. Shibata, S. Matsunami and T. Kakuchi, *Polymer*, 1996, **37**, 4435–4437.
29 M.-H. Lai, J. H. Jeong, R. J. DeVolder, C. Brockman, C. Schroeder and H. Kong, *Adv. Funct. Mater.*, 2012, **22**, 3239–3246.
30 W. H. Daly and D. Poché, *Tetrahedron Lett.*, 1988, **29**, 5859–5862.
31 D. A. Christian, S. Cai, D. M. Bowen, Y. Kim, J. D. Pajerowski and D. E. Discher, *Eur. J. Pharm. Biopharm.*, 2009, **71**, 463–474.
32 S. H. Wibowo, A. Sulistio, E. H. H. Wong, A. Blencowe and G. G. Qiao, *Aust. J. Chem.*, 2014, **67**, 598–602.
33 S. H. Wibowo, A. Sulistio, E. H. H. Wong, A. Blencowe and G. G. Qiao, *Chem. Commun.*, 2014, **50**, 4971.
34 H. Senn, B. Werner, B. A. Messerle, C. Weber, R. Traber and K. Wüthrich, *FEBS Lett.*, 1989, **249**, 113–118.
35 B. Dalhus, C. H. Görbitz, P. Kofod, E. Larsen, B. Nielsen, R. I. Nielsen, C. E. Olsen, C. N. Rosendahl, M. Haugg, N. Trabesinger-Rüf and E. G. Weinhold, *Acta Chem. Scand.*, 1996, **50**, 544–548.
36 Y. Geng and D. E. Discher, *J. Am. Chem. Soc.*, 2005, **127**, 12780–12781.
37 S. Rameez, I. Bamba and A. F. Palmer, *Langmuir*, 2010, **26**, 5279–5285.
38 P. J. Flory, *J. Chem. Phys.*, 1942, **10**, 51–61.
39 S. S. Jawalkar, K. V. S. N. Raju, S. B. Halligudi, M. Sairam and T. M. Aminabhavi, *J. Phys. Chem. B*, 2007, **111**, 2431–2439.

40 C. Zhang, B. Liu, X. Wang, H. Wang and H. Zhang, *J. Chem. Eng. Data*, 2014, **59**, 2732–2740.
41 X. Xiao, J. Hu, D. H. Charych and M. Salmeron, *Langmuir*, 1996, **12**, 235–237.
42 L. Capretto, D. Carugo, W. Cheng, M. Hill and X. Zhang, *J. Colloid Interface Sci.*, 2011, **357**, 243–251.
43 M. P. Schultz, J. A. Finlay, M. E. Callow and J. A. Callow, *Biofouling*, 2000, **15**, 243–251.
44 B. K. Johnson and R. K. Prud'homme, *Phys. Rev. Lett.*, 2003, **91**, 118302.
45 J. L. Santos and M. Herrera-Alonso, *Macromolecules*, 2014, **47**, 137–145.
46 M.-H. Lai, S. Lee, C. E. Smith, K. Kim and H. Kong, *ACS Appl. Mater. Interfaces*, 2014, **6**, 10821–10829.
47 H. Sun, *J. Phys. Chem. B*, 1998, **102**, 7338–7364.
48 S. Nosé, *J. Chem. Phys.*, 1984, **81**, 511–519.